AIP | Review of Scientific Instruments

Infrared imaging video bolometer

B. J. Peterson

Citation: Rev. Sci. Instrum. **71**, 3696 (2000); doi: 10.1063/1.1290044

View online: http://dx.doi.org/10.1063/1.1290044

View Table of Contents: http://rsi.aip.org/resource/1/RSINAK/v71/i10

Published by the American Institute of Physics.

Related Articles

Hydrogen transport diagnostics by atomic and molecular emission line profiles simultaneously measured for large helical device
Phys. Plasmas 20, 012514 (2013)

Time-and-space resolved comparison of plasma expansion velocities in high-power diodes with velvet cathodes
J. Appl. Phys. 113, 043307 (2013)

Development of a diffuse air-argon plasma source using a dielectric-barrier discharge at atmospheric pressure
Appl. Phys. Lett. 102, 033503 (2013)

Nonmonotonic radial distribution of excited atoms in a positive column of pulsed direct currect discharges in helium
Appl. Phys. Lett. 102, 034104 (2013)

Iterative Boltzmann plot method for temperature and pressure determination in a xenon high pressure discharge lamp
J. Appl. Phys. 113, 043303 (2013)

Additional information on Rev. Sci. Instrum.

Journal Homepage: http://rsi.aip.org

Journal Information: http://rsi.aip.org/about/about_the_journal

Top downloads: http://rsi.aip.org/features/most_downloaded

Information for Authors: http://rsi.aip.org/authors

ADVERTISEMENT

Infrared imaging video bolometer

B. J. Peterson[a)]
National Institute for Fusion Science, Toki-shi, Gifu-ken 509-5292, Japan

(Received 7 September 1999; accepted for publication 27 June 2000)

A new concept for an infrared imaging bolometer is proposed which provides full video (two-dimensional) imaging of the radiated power from the plasma. This concept preserves all the advantages (compared to conventional metal foil resistive bolometers) of the previously proposed and tested segmented mask infrared imaging bolometer (SIB). It avoids the problems associated with the copper mask of the SIB, while giving a full frame video image of the plasma radiation with improved experimental flexibility regarding the pixel size. Analysis of the noise equivalent power shows that compared to a SIB with the same pixel area, the infrared imaging video bolometer is 2–5 times more sensitive with improved spatial resolution. These benefits are gained at the expense of the mechanical support, which the mask provides for the foil in the SIB. A numerical algorithm is used to solve the two-dimensional heat diffusion equation for the foil and determine the time-dependent spatial distribution of incident power on the foil from the infrared (IR) video camera measurements of the foil temperature. Testing the algorithm using a Gaussian model of the incident power shows that it can accurately reproduce the Gaussian model to within 6%. A simple scheme to absolutely calibrate the entire foil is described and several design points are detailed pointing out the range and experimental flexibility of the diagnostic using currently available IR camera technology. © *2000 American Institute of Physics.* [S0034-6748(00)02310-8]

I. INTRODUCTION

Radiation plays an important role in the overall power balance of the plasma by cooling the plasma primarily at the edge. In early fusion experiments a single thermistor-backed metal foil bolometer with a 2π view was commonly used to estimate the total power radiated by the plasma.[1,2] The need for a more durable sensor that can endure high temperature baking and is impervious to damage from neutrons and gamma rays led to the development of a metal thermoresistor bolometer.[3–5] Miniaturization of these detectors has allowed them to be mounted in multiple arrays, which view the plasma in one poloidal cross section.[6] Tomographic analysis of the resulting data could be performed which provides a two-dimensional view of the radiated power.[7,8] The progress of magnetic fusion studies beyond the relatively simple axisymmetric magnetic configurations of tokamaks to the more complex, fully three-dimensional geometries of helical devices calls for the development of two-dimensional diagnostics which by means of the use of multiple cameras and advanced tomography can provide the necessary three-dimensional data. This motivated the development of a two-dimensional bolometer which takes advantage of recent advances in infrared imaging technology to replace the resistive measurement of the metal foil's temperature with an infrared measurement.[9]

II. INFRARED IMAGING BOLOMETERY

Infrared imaging bolometery originated with single detectors measuring the radiation from a single metal foil.[10,11] The use of an infrared (IR) camera to measure the foil temperature was first proposed in an article investigating the relationship between operating temperature, wavelength, and signal-to-noise ratio.[12] The concept of a two-dimensional IR imaging bolometer (IRIB) was introduced utilizing a two-dimensional segmented matrix of raised absorbers.[9] This evolved into the segmented mask infrared imaging bolometer (SIB), a two-dimensional array of metal foil pixels,[13] which was designed, constructed and tested on the compact helical system device[14] and is described below.

By sandwiching a thin metal foil between two identical copper masks having a two-dimensional hole pattern, a two-dimensional array of foil pixels exposed to both sides is formed as shown in Fig. 1. On the front side the array is exposed to the plasma through a pinhole or slit aperture. Meanwhile, an IR camera views the blackened backside of the foil array through an IR transmitting vacuum window, measuring the temperature rise of the foil pixels resulting from the radiation incident on the front side as seen in Fig. 2. The copper masks form a heat sink for each pixel, the size, thickness and thermal properties of which determine the steady-state sensitivity, K (in °C/W), and thermal diffusion time, τ of the pixel. Since the foil and mask are at high vacuum inside the vacuum vessel, there is no atmospheric cooling and the only cooling of the foil is from the mask. The mask should also thermally isolate the foil pixels from each other. The thickness of the foil, t_f is chosen to be able to stop the highest energy photon expected. The diameter of the pixel should be chosen such that the thermal diffusion time of the pixel matches the frame interval Δt of the camera. The relationship between the pixel diameter d_{pix} and its thermal diffusion time is given by Eq. (1) where κ is the thermal diffusivity of the foil material in m^2/s:

a)Electronic mail: peterson@LHD.nifs.ac.jp

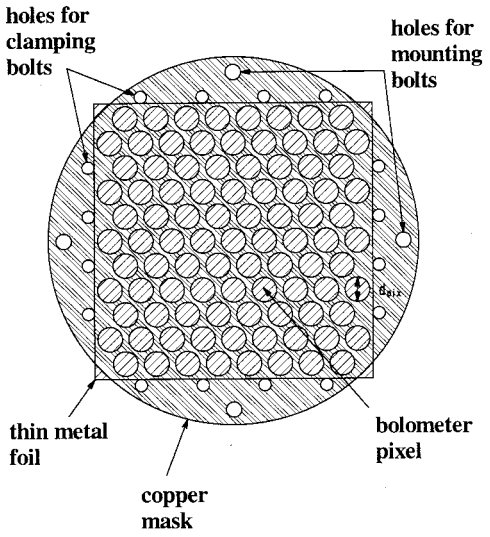

FIG. 1. Example of a mask and foil arrangement for a SIB.

$$\tau \propto \frac{d_{\mathrm{pix}}^2}{\kappa}. \tag{1}$$

If the pixel diameter is larger than this value the heat from this time slice will not dissipate before the next time slice, if it is smaller than this value the heat will dissipate too quickly. The spatial resolution is then determined by the aperture and camera geometry. Each pixel is calibrated by illuminating the blackened side with the chopped light of a helium-neon laser of known power and measuring the calibration parameters, τ and K (°C/W). The power to each pixel is then given by

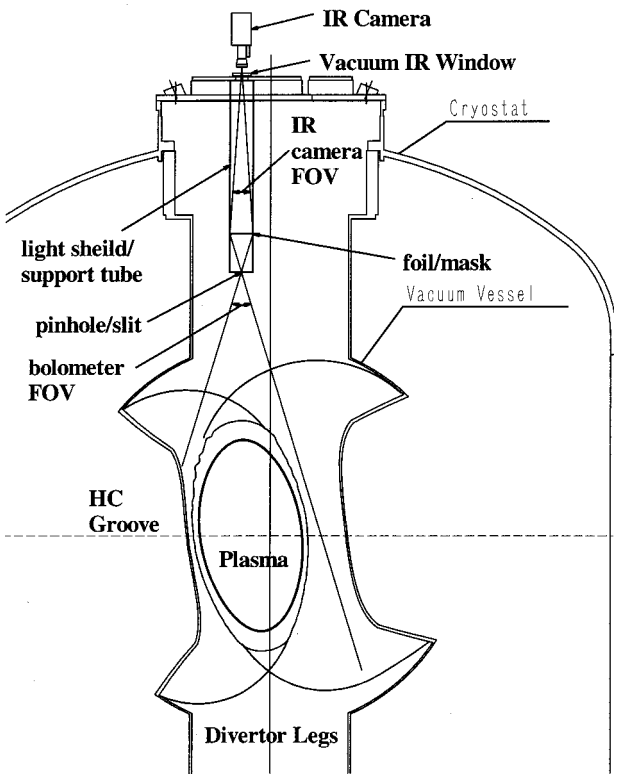

FIG. 2. Example of an IRIB installation in the large helical device.

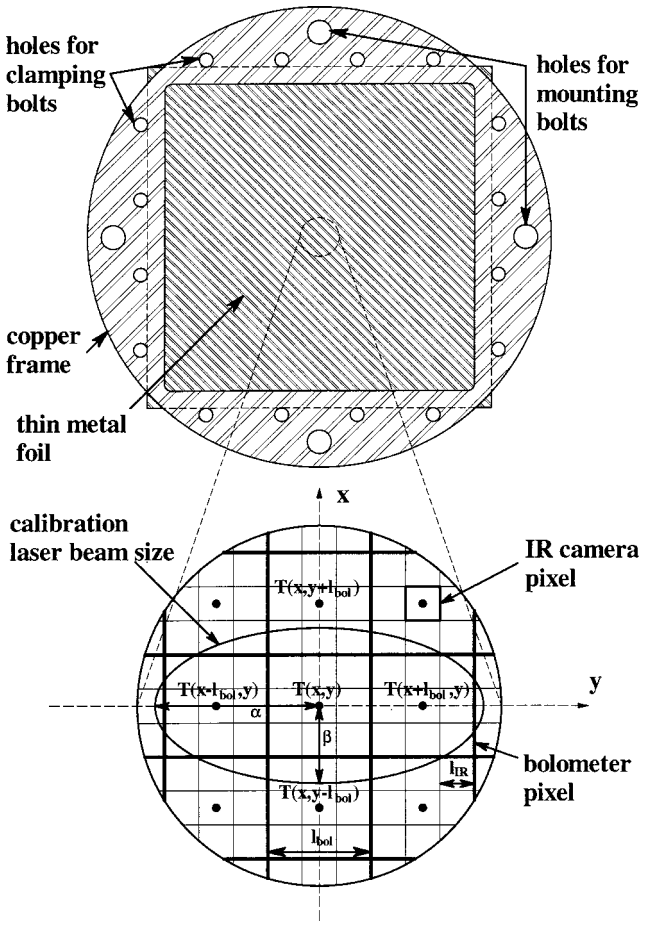

FIG. 3. Mask and foil arrangement for the IRVB showing geometry for FTCS algorithm.

$$P_{\mathrm{rad}} = \frac{1}{K}\left(T + \tau \frac{\partial T}{\partial t}\right), \tag{2}$$

with T the temperature of the foil with respect to the mask temperature, just as in the case of resistive metal film bolometers. Note that the calibration parameters, τ and K, can be written in terms of the heat capacity, c (J/°C), and thermal conductivity, k (W/m/°C), as $\tau = c/kt_f$ and $K = 1/t_f k$.

Some problems arise from the masks. First of all, dishing of the copper masks can result in poor contact of the copper heat sink to the foil at the pixel edge for some of the pixels resulting in ''cross talk'' due to heat flow between neighboring pixels. This may be partially solved by adding more clamping bolts between pixels at the expense of decreased pixel area. Another problem is shadowing of some portion of the pixels by the front side of the mask.

III. INFRARED IMAGING VIDEO BOLOMETER

A search for a solution to the problems of the SIB has given rise to a new concept in imaging bolometery, the infrared imaging video bolometer (IRVB). The IRVB differs from the SIB by eliminating the mask and using one large copper frame to support the entire foil as shown in Fig. 3. This increases the usable area of the foil by approximately 40% in the case of the designs shown in Figs. 1 and 3. The dishing problems of the masks mentioned above are avoided

as the contact of the copper frame and foil is ensured by the tightening screws near the edge of the frame and can be further improved by the use of an indium gasket. Also, the shadowing of the foil by the copper masks is avoided. The roles of the masks in the definition and thermal isolation of each pixel are no longer necessary as an algorithm has been developed which accounts for the thermal diffusion in the foil, which is described below. One disadvantage of the IRVB is the lack of support given to the foil by the SIB mask.

The fundamental difference between the SIB and the IRVB is in how they deal with the thermal diffusion in the foil. Instead of using the copper mask to physically divide the foil into thermally isolated circular pixels, the entire foil is numerically divided into square pixels of dimension l_{bol}, (designated ''bolometer pixels''). The length l_{bol} should be greater than or equal to the image size l_{IR} of the IR camera's pixels (designated ''IR pixels'') as shown in Fig. 3. The change in temperature ΔT of each bolometer pixel during Δt can be written as the sum of the temperature change due to diffusion, ΔT_{dif}, and the temperature change due to the incident power from the plasma radiation, ΔT_{rad},

$$\Delta T = \Delta T_{\mathrm{dif}} + \Delta T_{\mathrm{rad}}. \tag{3}$$

ΔT_{dif} for each bolometer pixel is determined by solving the two-dimensional heat diffusion equation in rectangular coordinates,

$$\frac{\partial^2 T}{\partial x^2} + \frac{\partial^2 T}{\partial y^2} = \frac{1}{\kappa}\frac{\partial T}{\partial t}, \tag{4}$$

where *T(x, y, t)* is the temperature of the foil at horizontal position, *x*, and vertical position, *y*, at time, *t*. In applying this equation to our foil using a forward time, center space (FTCS) algorithm,[15] it can be rewritten with $l = l_{\mathrm{bol}}$ as

$$\frac{T(x,y+l)+T(x,y-l)+T(x+l,y)+T(x-l,y)-4T(x,y)}{l^2} = \frac{\Delta T_{\mathrm{dif}}(x,y,t)}{\kappa \Delta t} \tag{5}$$

(geometry shown in Fig. 3) with the left-hand side evaluated at $t-\Delta t$. ΔT can be written as

$$\Delta T(x,y,t) = T(x,y,t) - T(x,y,t-\Delta t) \tag{6}$$

and ΔT_{rad} can be written in terms of the incident radiated power from the plasma P_{rad}, as

$$\Delta T_{\mathrm{rad}}(x,y,t) = \frac{P_{\mathrm{rad}}(x,y,t)\Delta t \kappa}{k t_f l^2}, \tag{7}$$

where k is the thermal conductivity of the foil. Solving for P_{rad} using Eqs. (3)–(7) gives

$$P_{\mathrm{rad}}(x,y,t) = t_f k \{ l^2 [T(x,y,t) - T(x,y,t-\Delta t)]/\kappa \Delta t + [4T(x,y) - T(x,y+l) - T(x,y-l) - T(x+l,y) - T(x-l,y)]_{t-\Delta t} \}. \tag{8}$$

The stability criterion for the FTCS algorithm is given by[16]

$$l_{\mathrm{bol}}^2 = l^2 \geqslant 2\kappa \Delta t \tag{9}$$

which can be used to determine the minimum value of l_{bol}. The temperature measurements of the IR pixels whose image makes up the bolometer pixel can be averaged to reduce the noise and improve the sensitivity. If necessary, depending on the signal level, the pixel size, l_{bol}, can be increased above the minimum to improve the signal-to-noise ratio at the cost of spatial and time resolution. This makes the IRVB more flexible than the previous masked version having a fixed pixel size.

IV. CALIBRATION

Due to possible nonuniformity in t_{f} from fabrication and in κ and k due to the carbon coating needed on the IR camera side of the foil, calibration is necessary. Equation (8) can be written in the form of Eq. (2) with

$$\tau = \frac{l_{\mathrm{bol}}^2}{\kappa} \quad \text{and} \quad K = \frac{1}{t_f k}. \tag{10}$$

Therefore, calibration can be carried out by determining these two quantities for each bolometer pixel. This is most effectively done by determining *K(x,y)* and $\tau(x,y)$ (that is, for each IR pixel) and then averaging those quantities over those IR pixels which make up the bolometer pixel. The thermal time τ can be measured by quickly heating the foil, then removing the heat source and measuring each pixel's temperature decay time. The sensitivity K of each IR pixel can be measured relatively by heating the foil with a uniform light source and measuring the temperature distribution at thermal equilibrium $[\partial T_{\mathrm{heat}}(x,y)/\partial t = 0]$. This distribution of the foil temperature with respect to the frame temperature is then compared with that of a perfectly uniform thin foil given by

$$T_{\mathrm{rel}}(x,y) = \frac{16 S_{\mathrm{heat}} K}{\pi^2} \sum_{m=0}^{\infty} \sum_{l=0}^{\infty} \frac{\cos \lambda_l x \cos \lambda_m y}{(2l+1)(2m+1)\lambda_{lm}^2}, \tag{11}$$

where

$$\lambda_l = \frac{(2l+1)\pi}{a}, \quad \lambda_m = \frac{(2m+1)\pi}{b}, \quad \lambda_{lm} = \sqrt{\lambda_l^2 + \lambda_m^2} \tag{12}$$

and where the edge of the foil is at $x = \pm a/2$, $y = \pm b/2$, and S_{heat} is the unknown power density of the uniform heat source at the foil. Equation (11) was derived by analytically solving the heat diffusion equation in rectangular coordinates given by Eq. (4) using a uniform power distribution, S_{heat}, divided by k, as the boundary condition for the first derivative of the temperature in the z direction. Since S_{heat} is unknown, the ratio of the measured temperature to this temperature distribution is normalized to the center IR pixel of the foil giving the relative calibration of each pixel:

$$K_{\mathrm{rel}}(x,y) = \frac{T_{\mathrm{heat}}(x,y)}{T_{\mathrm{rel}}(x,y)}. \tag{13}$$

The absolute calibration can be carried out by illuminating the center of the foil with a light source of a known

power distribution. For instance, if a helium–neon laser of a known power P_{laser} with a Gaussian power distribution given by

$$S_{\text{laser}}(x,y)=\frac{P_{\text{laser}}}{\pi(\alpha^2+\beta^2)}\exp[-(x^2/\alpha^2+y^2/\beta^2)], \quad (14)$$

with beam radii of α and β in the x and y directions, respectively, is used to illuminate the center of the foil starting at $t=0$,, the resulting temperature evolution near the center of the foil is given by

$$T_{\text{laser}}(x,y,t)=\frac{4\alpha\beta K(x,y)P_{\text{laser}}}{ab(\alpha^2+\beta^2)} \times\sum_{m=0}^{\infty}\sum_{l=0}^{\infty}\frac{\cos\lambda_l x\cos\lambda_m y}{\lambda_{lm}^2} \times e^{-(\alpha^2\lambda_l^2+\beta^2\lambda_m^2)/4}(1-e^{-\kappa\lambda_{lm}^2 t}) \quad (15)$$

for $\alpha,\beta\ll a,b$. This relation has been derived by analytically solving the heat diffusion equation in rectangular coordinates given by Eq. (4) using the Gaussian function given as Eq. 14 divided by k, as the boundary condition for the first derivative of the temperature in the z direction. Taking the temporal limit of this as the foil reaches thermal equilibrium ($t=\infty$) and integrating this over the IR pixel and dividing by its area gives the temperature of the center IR pixel T_{center}:

$$T_{\text{center}}=\frac{4\alpha\beta K_{\text{center}}P_{\text{laser}}}{ab(\alpha^2+\beta^2)} \times\sum_{m=0}^{\infty}\sum_{l=0}^{\infty}\frac{\exp[-(\alpha^2\lambda_l^2+\beta^2\lambda_m^2)/4]}{\lambda_{lm}^2} \times\left[1-\frac{l_{\text{IR}}^2\lambda_{lm}^2}{24}+\frac{l_{\text{IR}}^4\lambda_l^2\lambda_m^2}{24^2}\right]. \quad (16)$$

Solving Eq. (16) for K_{center} one can determine the absolute calibration, *K(x,y)*:

$$K(x,y)=K_{\text{center}}K_{\text{rel}}(x,y). \quad (17)$$

V. THERMAL MODELING OF THE FOIL

Using the equations introduced above, modeling is carried out to investigate the accuracy of the FTCS algorithm in giving the incident power on the foil. First of all, the incident power on the foil is modeled as a Gaussian function as given by Eq. (14) and shown by the solid line in Fig. 4 with $P_{\text{laser}}=20$ mW and $\alpha=\beta=4$ mm. This choice of a Gaussian function is arbitrary and chosen out of convenience. The power density level of the model is on the order of that expected from a typical fusion plasma (10 mW/cm^2). Then the resulting foil temperature distribution evolution is calculated using Eq. (15) with 70 Fourier terms used in each dimension. For the purposes of this study a uniform gold foil is assumed ($a=b=9$ cm, $t_f=1$ μm, $k=3.16$ W/cm °C, $\kappa=1.27$ cm^2/s). An example of the temperature distribution evolution during the first ten time steps is shown in Fig. 5 for the case where $\Delta t=4$ ms. The temperature levels for this case are well above the sensitivity of current infrared cameras (25–100 m °C). Finally, using this temperature distribution evolution the incident power distribution is calculated by the FTCS algorithm using Eq. (8) for $l_{\text{bol}}=1$ mm as given by Eq. 9. The result is shown by the dashed line in Fig. 4. This calculated distribution varies from the original distribution (in this case Gaussian) by less than 6** at its peak demonstrating the ability of the FTCS algorithm to accurately reproduce the incident power profile.

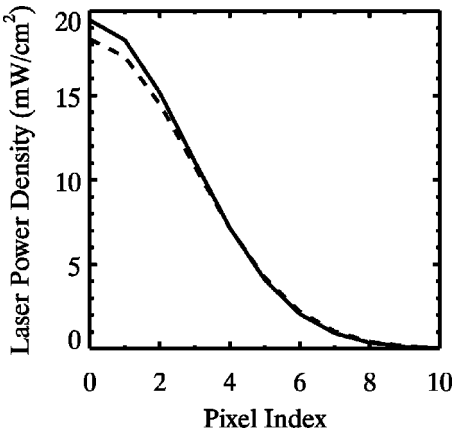

FIG. 4. Plot of Gaussian model of incident power density profile (solid line) and result of FTCS algorithm calculation (broken line).

VI. NOISE EQUIVALENT POWER CALCULATIONS

In this section expressions for the noise equivalent power (NEP) for both the SIB and the IRVB are derived and compared. NEP is a figure of merit for bolometers indicating the signal power level when the signal to noise ratio, $S/N=1$. Therefore, a lower NEP results in a more sensitive measurement.

Starting with the SIB we take Eq. (1) from Ref. 1 and let $S_f=P_{\text{rad}}/\pi b^2$, where b is the pixel radius. Integrating this temperature equation over the pixel area and dividing by the area results in the average temperature over the pixel

$$T_{\text{avg}}(t)=\frac{4}{\pi b^4}\frac{P_{\text{rad}}}{kt_f}\sum_{m=1}^{\infty}\frac{1-\exp[-\kappa\beta_m^2 t]}{\beta_m^4}, \quad (18)$$

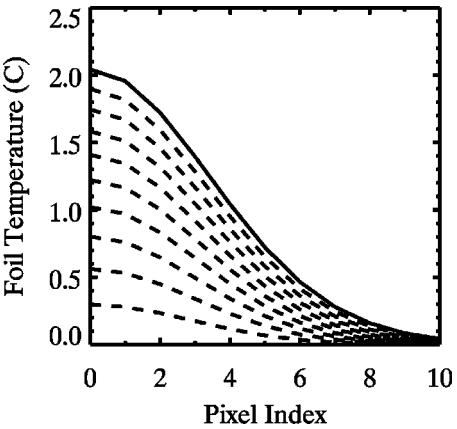

FIG. 5. Time evolution of foil temperature profile during the first ten time steps of the model. Temperature profile is initially zero and rises to the profile shown by the solid line at $t=10\Delta t$. This data is used for the FTCS calculation whose result is shown in Fig. 4.

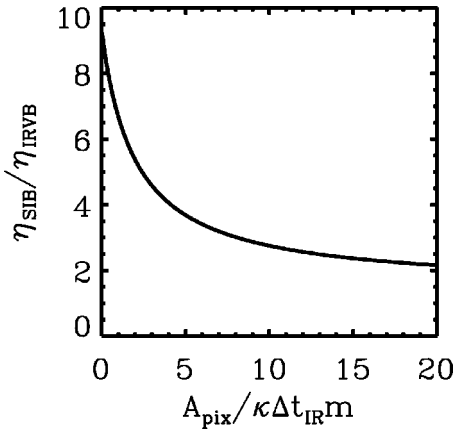

FIG. 6. Ratio of NEP values for the SIB and the IRVB, $\eta_{\mathrm{SIB}}/\eta_{\mathrm{IRVB}}$, versus $A_{\mathrm{pix}}/\kappa\Delta t_{\mathrm{IR}}m$ assuming the same pixel size and foil material.

where $\beta_m=\alpha_m/b$ and α_{m} are the zeros of the Bessel function of the first kind of zero order. The use of the Bessel function stems from the circular geometry of the pixel. Ignoring all but the first term of the series this can be written as

$$T_{\mathrm{avg}}(t)=KP_{\mathrm{rad}}[1-\exp(-t/\tau)]. \tag{19}$$

This can be rewritten in the form of Eq. (2) with $K=4/\pi\alpha_1^4 kt_f$ and $\tau=b^2/\kappa\alpha_1^2$. Expressing the error in T_{avg}, σ_T, in terms of the error in the IR camera measurement, σ_{IR}, and the number of IR pixels, N_{IR}, composing one bolometer pixel as $\sigma_T=\sigma_{\mathrm{IR}}/\sqrt{N_{\mathrm{IR}}}$ and applying standard error analysis,[16] the noise equivalent power η can be written in the form

$$\eta_{\mathrm{SIB}}=\frac{\pi\alpha_1^4}{4}kt_f\frac{\sigma_{\mathrm{IR}}}{\sqrt{mN_{\mathrm{IR}}}}\left(\frac{\sqrt{2}}{\alpha_1^2\pi}\frac{A_{\mathrm{pix}}}{\kappa\Delta t_{\mathrm{IR}}m}+1\right), \tag{20}$$

where Δt_{IR} is the frame interval of the IR camera, m is the number of frames over which the signal is averaged (resulting in a time resolution for the diagnostic of $\Delta t=m\Delta t_{\mathrm{IR}}$) and $A_{\mathrm{pix}}=\pi b^2$ is the area of the bolometer pixel. This analysis assumes that there is no error in the measurement of the mask temperature. If one chooses to not make this assumption and averages over the same number of IR camera pixels to find the mask temperature as are used to find the pixel temperature, the NEP of the SIB will increase by a factor of $\sqrt{2}$. For the IRVB, applying error analysis to Eq. (8) one arrives at a NEP of

$$\eta_{\mathrm{IRVB}}=2\sqrt{2}kt_f\frac{\sigma_{\mathrm{IR}}}{\sqrt{mN_{\mathrm{IR}}}}\left(\frac{1}{2}\frac{A_{\mathrm{pix}}}{\kappa\Delta t_{\mathrm{IR}}m}+1\right). \tag{21}$$

In order to compare the NEP values for the SIB and IRVB, the ratio of NEP values, $\eta_{\mathrm{SIB}}/\eta_{\mathrm{IRVB}}$, is plotted in Fig. 6 as a function of $A_{\mathrm{pix}}/\kappa\Delta t_{\mathrm{IR}}m$, a dimensionless quantity that is the ratio of the bolometer pixel area to the area through which heat will diffuse in the time $\Delta t_{\mathrm{IR}}m$. The lower limit of two for this ratio is given by the stability criterion for the FTCS algorithm in Eq. (9). This shows that for any value of $A_{\mathrm{pix}}/\kappa\Delta t_{\mathrm{IR}}m$ the IRVB is more sensitive than the SIB. For the range of practical interest ($2<A_{\mathrm{pix}}/\kappa\Delta t_{\mathrm{IR}}m<20$) the IRIB is 5–2 times more sensitive than a SIB having the same pixel size (area). This improvement in sensitivity results because the mask cools the foil locally and therefore reduces the average temperature over the pixel and thus the signal level of the SIB. In addition to the improved sensitivity of the IRVB over the SIB of the same pixel size, the IRVB will also have better spatial resolution. This is due to the increase in the number of IR pixels viewing the foil area which was occupied by the mask in the case of the SIB. For example, taking the geometries shown in Figs. 1 and 3, the IRVB can fit 14% more pixels in each dimension than the SIB having the same pixel size and foil size. Therefore, regardless of the foil material and mask geometry, the IRVB is always more sensitive and has better spatial resolution than a SIB having the same pixel size.

VII. DESIGN CONFIGURATION FLEXIBILITY

One of the features of the IRVB is the flexibility of the diagnostic to allow tradeoffs between sensitivity, spatial, and time resolution without the need to change the foil frame. This can be seen in Table I where the details of several experimental configurations are shown for three different infrared cameras using the same foil. The first entry shows that with a state of the art camera one can obtain tens of thousands of channels of data at millisecond resolutions with a

TABLE I. Six different operating configurations for three different camera specifications using the same foil/frame. Δt_{IR} is the frame interval of the IR camera. Noise equivalent power density, $\eta_{\mathrm{IRVB}}/A_{\mathrm{pix}}$, is given for the case of a gold foil, $t_f=1$ μm, $k=3.16$ W/cm °C, $\kappa=1.27$ cm^2/s and an IR camera sensitivity of $\sigma_{\mathrm{IR}}=25$ m °C.

IR camera parameters			Bolometer parameters				Noise reduction			
Δt_{IR}	l_{IR}	pixel/side	Δt	l_{bol}	Pixel/side	$\frac{\eta_{\mathrm{IRVB}}}{A_{\mathrm{pix}}}$	Time avg	Pixel avg	Total ΔS/N	
(ms)	(mm)		(ms)	(mm)		$\left(\frac{\mu W}{\mathrm{cm}^2}\right)$	$\sqrt{\frac{\Delta t}{\Delta t_{\mathrm{IR}}}}\times\frac{l_{\mathrm{bol}}}{l_{\mathrm{IR}}}=\Delta\frac{S}{N}$			$\frac{\eta_{\mathrm{SIB}}}{\eta_{\mathrm{IRVB}}}$
1	0.35	256	1	0.5	180	31.6	1	1.4	1.4	5.40
1	0.35	256	4	1.0	90	7.6	2	2.9	5.8	5.40
1	0.35	256	10	1.6	56	3.1	3.3	4.5	14.4	5.35
16.7	0.35	256	16.7	2.1	45	7.7	1	5.9	5.9	5.29
33.3	1.32	68	33.3	2.9	31	20.2	1	2.2	2.2	5.38
33.3	1.32	68	100	5.0	18	6.7	1.7	3.8	6.6	5.40

sensitivity of 30 μW/cm^2. The next two entries show the gains that can be made in sensitivity by noise reduction through sample and pixel averaging at the expense of temporal and spatial resolution using the same camera (the second entry is the case used in the previous section). The last three entries show that even for lower performance cameras hundreds of channels can be observed with reasonable sensitivity although at slower time resolutions. One can see that it is most advantageous to use a high speed camera with a large number of pixels in order to take advantage of time sample averaging and pixel averaging to improve the sensitivity through noise reduction. In the right hand column of Table I the ratio of NEP values are shown for each configuration for a gold foil. For each of the six configurations the IRVB is over 5 times more sensitive than a SI having the same pixel size.

VIII. DISCUSSION

In addition to the advantages mentioned above a possible disadvantage of the IRVB compared to the SIB is the relative lack of support for the foil that was previously provided by the mask. Therefore, care must be taken to avoid air pressure differences between the two sides of the foil through vents in the frame. If necessary, this may be compensated for by using a mylar backed foil. While this may have an effect on the thermal properties of the foil, they can be accounted for in the calibration scheme described above. Also, this support issue will become less important as thicker foils will be needed to stop the higher energy photons from a reactor-grade plasma. In addition to the two-dimensional absolute quantitative measurement of the radiated power using the algorithm described above, the IRVB also can provide a qualitative real-time video image of the radiated power from present and future steady-state fusion devices.

ACKNOWLEDGMENTS

The author would like to thank Dr. Glen Wurden of Los Alamos National Laboratory for comments on this article and his sharing with me many ideas regarding infrared imaging bolometery. He would also like to thank Professor S. Sudo and Professor M. Fujiwara of NIFS for their encouragement of this work.

[1] H. J. Karr, E. A. Knapp, and J. E. Osher, Phys. Fluids **4**, 424 (1961).
[2] H. Hsuan, K. Bol, and R. A. Ellis, Nucl. Fusion **15**, 657 (1975).
[3] G. Miller, J. C. Ingraham, and L. S. Schrank, Rev. Sci. Instrum. **53**, 1410 (1982).
[4] J. Schivell, G. Renda, J. Lowrance, and H. Hsuan, Rev. Sci. Instrum. **53**, 1527 (1982).
[5] E. R. Mueller and F. Mast, J. Appl. Phys. **55**, 2635 (1984).
[6] K. F. Mast *et al.*, Rev. Sci. Instrum. **62**, 744 (1991).
[7] A. W. Leonard *et al.*, Rev. Sci. Instrum. **66**, 1201 (1995).
[8] L. Giannone *et al.*, Rev. Sci. Instrum. **68**, 762 (1995).
[9] G. A. Wurden, in *Diagnostics for Experimental Thermonuclear Fusion Reactors*, edited by P. E. Stott *et al.* (Plenum, New York, 1996), pp. 603–606.
[10] TFR Group (presented by A. L. Pecquet), J. Nucl. Mater. **93–94**, 377 (1980).
[11] J. C. Ingraham and G. Miller, Rev. Sci. Instrum. **54**, 673 (1983).
[12] G. Apruzzese and G. Tonini, Rev. Sci. Instrum. **61**, 2976 (1990).
[13] G. A. Wurden, B. J. Peterson, and S. Sudo, Rev. Sci. Instrum. **68**, 766 (1997).
[14] G. A. Wurden and B. J. Peterson, Rev. Sci. Instrum. **70**, 255 (1999).
[15] W. H. Press *et al.*, *Numerical Recipes, the Art of Scientific Computing* (Cambridge University Press, Cambridge, 1986), pp. 635–642.
[16] P. R. Bevington and D. K. Robinson, *Data Reduction and Error Analysis for the Physical Sciences* (McGraw-Hill, Boston, MA, 1992), pp. 38–52.